

Toward Real-time Analysis of Experimental Science Workloads on Geographically Distributed Supercomputers

Michael Salim

msalim@anl.gov

Argonne National Laboratory

Lemont, Illinois, USA

Thomas Uram

turam@anl.gov

Argonne National Laboratory

Lemont, Illinois, USA

J. Taylor Childers

jchilders@anl.gov

Argonne National Laboratory

Lemont, Illinois, USA

Venkat Vishwanath

venkat@anl.gov

Argonne National Laboratory

Lemont, Illinois, USA

Michael E. Papka

papka@anl.gov

Argonne National Laboratory

Lemont, Illinois, USA

ABSTRACT

Massive upgrades to science infrastructure are driving data velocities upwards while stimulating adoption of increasingly data-intensive analytics. While next-generation exascale supercomputers promise strong support for I/O-intensive workflows, HPC remains largely untapped by live experiments, because data transfers and disparate batch-queueing policies are prohibitive when faced with scarce instrument time. To bridge this divide, we introduce Balsam: a distributed orchestration platform enabling workflows at the edge to securely and efficiently trigger analytics tasks across a user-managed federation of HPC execution sites. We describe the architecture of the Balsam service, which provides a workflow management API, and distributed sites that provision resources and schedule scalable, fault-tolerant execution. We demonstrate Balsam in efficiently scaling real-time analytics from two DOE light sources simultaneously onto three supercomputers (Theta, Summit, and Cori), while maintaining low overheads for on-demand computing, and providing a Python library for seamless integration with existing ecosystems of data analysis tools.

1 INTRODUCTION

Department of Energy (DOE) supercomputers have been successfully leveraged by scientists for large-scale simulation in diverse fields, from understanding the evolution of the universe to discovering new materials. With the rise of two recent phenomena, this landscape is changing to include high-throughput computing (HTC) workloads, typically comprising a large collection of jobs with a mix of interdependencies that govern the concurrency available to be exploited. The first of these phenomena is the rise of artificial intelligence involving traditional machine learning or deep neural networks, which rely on large datasets to train models and reach levels of predictive accuracy making them useful on their own or in cooperation with traditional simulations. The second phenomenon emerges from data-intensive science, represented in the current work by experimental science: a range of experimental facilities are undergoing upgrades, or have recently completed upgrades, that will increase their data-taking rate, in some cases by as much as two orders of magnitude [12, 16, 26]. This change necessitates access to computing resources beyond the experimental facility [15, 21], in a manner that is reliable and flexible, to accommodate the real-time demands of the experiments, and the dynamic availability of

remote computing resources. These features, among others, have been explored in a variety of past workflow systems [8], job description approaches [20], and methods of mapping jobs to compute resources [11].

Computational workloads from experimental facilities are uniquely driven by their coupling to ongoing experiments, leading to these features: *significant data rates* that vary over time, from constant to bursty, depending on experiment specifics; the need for *near real-time processing* to inform researchers operating the experiment to maximize the scientific utility of the instrument; and *increasing fidelity in their analyses*, essential to analysis of the larger data emitted from experiments at upgraded facilities. These requirements have implications for networking between experimental and computing facilities, for queue depth on supercomputers, and for optimizing throughput. Workflows that bridge these facilities will open new opportunities for larger, higher-resolution, near real-time analyses that are critical in the face of expanding data rates. This paper describes the development of Balsam to meet these challenges, focusing particularly on the second.

Our development of Balsam aims to satisfy these needs with implementation in a few key areas: an application programming interface (API) for remote access to supercomputing facilities; close interaction with job schedulers to inject jobs opportunistically and bundle as ensembles to maximize throughput; interaction with data transfer mechanisms to move input (output) data to (from) remote locations, bundling transfers as needed; user-domain deployment, simplifying deployment while adhering to security requirements; and, distribution of jobs across multiple compute facilities simultaneously, with direction to a specific facility based on job throughput.

We demonstrate this functionality in the context of jobs flowing from two experimental facilities, the Advanced Photon Source (APS) at Argonne National Laboratory and the Advanced Light Source (ALS) at Lawrence Berkeley Laboratory, to three DOE compute facilities, the Argonne Leadership Computing Facility (ALCF), the Oak Ridge Leadership Computing Facility (OLCF), and NERSC. Balsam *sites* were deployed at each facility to bridge the site scheduler to the Balsam service. The central Balsam service exposes an API for introducing jobs and acts as a distribution point to the registered Balsam sites. Using the API, jobs were injected from the light source facilities simultaneously, executed at the computing sites, and results returned to the originating facility. Monitoring capabilities provide insight into the backlog at each Balsam site and,

therefore, a basis for making scheduling decisions across compute facilities to optimize throughput.

Lastly, while the current work emphasizes light source workloads, Balsam is easy to adopt and agnostic to applications, making this approach immediately applicable to other scientific applications and domains with similar requirements.

2 RELATED WORK

Workflow management framework (WMF) development has a rich history and remains an active field of research and development. Balsam focuses on orchestrating work submitted from remote users and run on multiple HPC sites. Here contemporary WMFs are discussed and contrasted.

funcX [13] users compose workflows from Python function building blocks, invoking functions in remote containers as an example of the function-as-a-service (FaaS) paradigm. funcX endpoints, which are similar to Balsam *sites* (3.2), run on the login nodes of target HPC resources where Globus Auth is used for authentication and user-endpoint association. These endpoints use ZeroMQ to communicate with a central funcX web service used by all funcX users. Jobs can be submitted via a remote client from any location. The funcX model advocates workflows comprised of functions which execute in containerized workers running on independent compute nodes. By contrast, the Balsam data model allows resource requirements (e.g. multi-node jobs with variable GPUs per MPI rank) to be specified as part of the job definition. funcX relies on complementary technologies, such as Parsl execution providers to provision resources and Globus Automate to orchestrate data transfers. Balsam includes these functionalities as part of the user site agent, bearing more in common to Fireworks in this regard.

Fireworks [17] manages user workflows stored in a persistent database server executed in local or remote run pilot payloads. Data staging has builtin support via `sftp`. Users deploy independent database as needed, designing workflows in YAML, JSON, or Python. Job submission is controlled by the database access controls.

Balsam is a Python-based WMF composed of a centralized server with clients running on HPC resources communicating with a message queue service and a persistent central database [22]. This enabled multi-site submission of many large HPC jobs. Further updates added support for aggregating many small jobs into single batch submissions [18]. There is builtin support for data staging via `sftp`, `ssh`, `http` and Globus, similar to Balsam.

RADICAL [10] manages workflow execution on remote compute resources using a message queue service. Users write their workflow in Python, including calls to the management API, which submits pilot jobs via `ssh` to the HPC scheduler. The manager and pilots communicate via the message queue setup by the user prior to execution. This is somewhat different from Fireworks and Balsam with their persistent central services.

Swift [25] is a Java-based WMF that defines a custom scripting language to write parallel workflows on clusters. Swift workflows are executed at the command line with no database or central service. Remote job submission is achieved via direct scheduler submission via `ssh` commands requiring password-less authentication.

Parsl [9] is a Python-based WMF in which users define their applications and workflows in Python, similar to funcX. Communication is supported via Python function parameters and shared file-systems. Data staging is native to Parsl with support for `ftp`, `ssh`, `http`, and Globus. Remote job submission to a supercomputer is not a focus of Parsl.

Dask [14] is a popular WMF employed in the private and public sectors. Users develop parallel algorithms in Python using tools from the Dask library including parallel extensions to common data structures and libraries, i.e. `numpy`, `pandas`, and `scikit-learn`. Dask focuses on easy development of in situ distributed algorithms for HPC.

Dask, Parsl, Swift, and funcX are similar in that they provide a *programming model* to the user, and the user benefits from implementing their workflows in the language of the framework. This is in contrast to Fireworks, Balsam, RADICAL, and Balsam, where the focus is on providing the underlying infrastructure and “workflow primitives” to run high-throughput campaigns efficiently and portably across diverse HPC computing architectures.

3 IMPLEMENTATION

Balsam (Figure 1) provides a centralized service allowing users to register execution *sites* from any laptop, cluster, or supercomputer on which they wish to invoke computation. The sites run user agents that orchestrate workflows locally and periodically synchronize state with the central service. Users trigger remote computations by submitting jobs to the REST API, specifying the Balsam execution site and location(s) of data to be ingested.

3.1 The Balsam Service

Balsam provides a centrally-hosted multi-tenant web application, enabling users to manage distributed Balsam sites and orchestrate workflows within or across sites. While the Balsam service issues access tokens and tracks users internally, user authentication is a modular plug-in, i.e. we have implemented generic Authorization Code and Device Code OAuth2 flows [3] permitting users to securely authenticate with an external OAuth2 provider. The Device Code flow enables secure login from browserless environments such as supercomputer login nodes. In the near future, we anticipate integrating with the federated identity management system implemented in the DOE distributed data and computing ecosystem (DCDE) [19]. While outside the scope of the present work, universal adoption of federated authentication/authorization protocols will facilitate the adoption of centralized services such as Balsam across DOE cyberinfrastructure.

The Balsam service drives a PostgreSQL [4] relational database that maintains the state of all workflows executing across user sites. The service exposes a REST API frontend to clients including users and *user agents* that drive the execution of workflows on HPC resources.

3.2 The Balsam Site

The Balsam site is a user-owned endpoint for remote execution of workflows. Sites are uniquely identified by a hostname and path to a *site directory* mounted on the host. The site directory is a self-contained project space for the user, which stores configuration

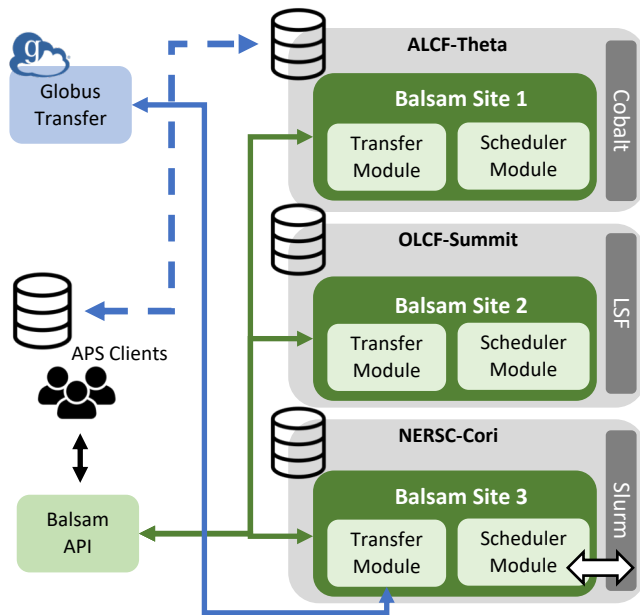


Figure 1: Simplified Balsam architecture. In this example scenario, clients at the Advanced Photon Source (APS) submit scientific workloads through the Balsam REST API. Balsam sites running on the ALCF-Theta, OLCF-Summit, and NERSC-Cori supercomputers communicate with the central API service to orchestrate out-of-band data transfers via Globus and to provision resources with the local batch scheduler.

data, application definitions, and a sandboxed directory where remote datasets are staged into *per-task* working directories prior to execution.

As part of its security model, Balsam does not permit direct injection of arbitrary commands or applications through its API. Instead, users write *ApplicationDefinition* classes in Python modules stored inside the site directory. These modules serve as flexible templates for the permissible workflows that may run at each Balsam site. **Balsam apps** registered with the API merely index the *ApplicationDefinitions* in each site with a 1:1 correspondence.

A **Balsam job** represents a single invocation of an app at a particular site. The job contains application-specific parameters (such as command line arguments), resource requirements (like the number of compute nodes or MPI ranks per node), and locations of data to be staged in or out before/after app execution. Users populate workflows by submitting Balsam jobs to the API. Each job references a specific app and is therefore bound to run at a single site upon creation. Jobs carry persistent state and metadata events generated from events throughout their lifecycle.

Each Balsam site runs an authenticated user agent that communicates with the central service to fetch jobs, orchestrate the workflow locally, and update the centralized state. The Balsam site agent is a collection of independent configurable modules that run as background processes on a host with gateway access to the site's

filesystems and HPC scheduler (e.g. an HPC login node). These modules are Python components written with the Balsam SDK, which uses locally stored access tokens to authenticate and exchange data with the REST API services.

The Balsam modules are architected to avoid hardcoding platform-dependent assumptions and enable facile portability across HPC systems. Indeed, the majority of Balsam component implementations are platform-independent, and interactions with the underlying diverse HPC fabrics are encapsulated in classes implementing uniform *platform interfaces*. Below we touch on a few of the key Balsam site modules and the underlying platform interfaces:

3.2.1 The Transfer Module. The Balsam transfer module queries the API service for pending *transfer items*, which are files or directories that need to be staged *in* or *out* for a particular Balsam job. The module batches transfer items between common endpoints and issues transfer tasks to the underlying transfer interface. For instance, the Globus transfer interface enables seamless interoperation of Balsam with Globus Transfer for dispatching out-of-band transfer tasks. The transfer module registers transfer metadata (e.g. Globus task UUIDs) with the Balsam API and polls the status of transfer tasks, synchronizing state with the API.

3.2.2 The Scheduler Module. The scheduler module uses an underlying scheduler platform interface to query local batch scheduler queues and submit resource allocations for pilot job launcher execution onto the queue. Interfaces to Slurm, Cobalt and LSF are provided to support DOE office of science supercomputing systems at NERSC, ALCF, and OLCF, respectively. The interface provides the necessary abstraction and enables one to easily support other schedulers. The Balsam scheduler module periodically checks on batch jobs submitted from the local site and synchronizes with state in the Balsam batch job API. For instance, users may provision resources through the Python SDK by remotely creating *BatchJob* resources with specified resources and queuing policies. The scheduler module fetches newly created *BatchJobs* from the Balsam API and submits them onto the local queues.

3.2.3 The Elastic Queue Module. A separate concern is automating queue submission: in real-time computing scenarios, users may wish to allow the site to automatically scale resources to a workload with resource requirements that vary over time. The elastic queue module allows users to configure minimum and maximum resource allocation sizes and dynamically creates batch jobs within these constraints to fit the resource requirements of the current workload size.

3.2.4 The Balsam Launcher. The Balsam launcher is a general pilot job mechanism that enables efficient and fault-tolerant execution of Balsam jobs across the resources allocated within an HPC batch job. The pilot job establishes an execution *session* with the service, which requires sending a periodic heartbeat signal to maintain a lease on acquired jobs. The session backend guarantees that concurrent launchers executing jobs from the same site do not acquire and process overlapping jobs. It further ensures that critical faults causing ungraceful launcher termination do not cause jobs to be locked in perpetuity: the stale heartbeat is detected by the service and affected jobs are reset to allow subsequent restarts. Launchers

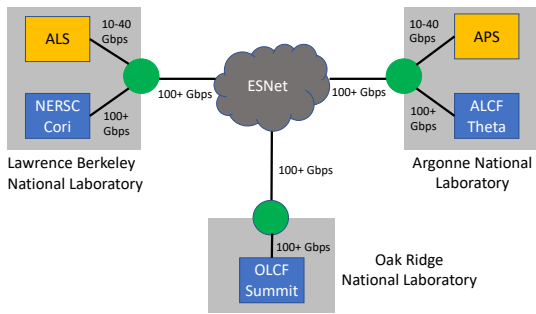


Figure 2: Connectivity between the geographically distributed Balsam sites (Theta at ALCF, Cori at NERSC, Summit at OLCF) and X-ray sources (APS at Argonne, ALS at LBNL). All networks are interconnected via ESNet.

rely on two platform interfaces: the *ComputeNode* interfaces defines available cores, GPUs, and MAPN (multiple applications per node) capabilities for the platform’s compute nodes. The *AppRun* interface abstracts the application launcher, and is used to execute applications in an MPI implementation-agnostic fashion.

4 EVALUATION

In this section, we evaluate the performance characteristics of Balsam in remote workload execution and ability to dynamically distribute scientific workloads among three DOE supercomputing platforms. We study two benchmark workflows in which a *full round-trip analysis* is performed: data is first transferred from a client experimental facility to the supercomputer’s parallel file system, computation on the staged data occurs on dynamically provisioned nodes, and results are finally transferred back from the supercomputer to the client’s local file system.

Our experiments address the following questions: (1) How effectively does scientific throughput scale given the real-world overheads in wide-area data transfers and in Balsam itself? (2) Is the total round-trip latency consistently low enough to prove useful in *near real-time* experimental analysis scenarios? (3) Does Balsam complete workloads reliably under conditions where job submission rates exceed available computing capacity and/or resources become unavailable mid-run? (4) Can *simultaneously provisioned* resources across computing facilities be utilized effectively to distribute an experimental workload in real-time? (5) If so, can the Balsam APIs be leveraged to adaptively map jobs onto distributed resources to improve overall throughput?

4.1 Methodology

4.1.1 Systems. Figure 2 depicts the geographically distributed supercomputing systems comprising of: a) **Theta [6]:** A Cray XC40 system at the ALCF, with 4392 compute nodes, having 64 1.3 GHz Intel Xeon Phi (Knight’s Landing) cores per node each with 192 GB memory. b) **Summit [5]:** An IBM AC922 system at the OLCF with 4,608 nodes, each node with two IBM Power 9 processors and six Nvidia V100 GPUs together with 512GB DDR4 and 96GB HBM2 memory. c) **Cori (Haswell Partition) [1]:** The Haswell partition of

Cori, a Cray XC40 system at NERSC, consists of X nodes each with two 2.3 GHz 16-core Intel Haswell processor with 128 GB memory.

The APS light source is located at Argonne and the ALS at LBNL. All three sites are interconnected via ESNet.

4.1.2 Balsam. The Balsam service, comprising both relational database and web server frontend, was deployed on a single AWS t2.xlarge instance. For the purpose of this experiment, user login endpoints were disabled and JWT authentication tokens were securely generated for each Balsam site. Moreover, inbound connectivity was restricted to traffic from the ANL, ORNL, and NERSC campus networks.

Three Balsam sites were deployed across the login nodes of Theta, Summit, and Cori. Balsam managed data transfers via the Globus Online [2] interface, between each compute facility and data transfer nodes at the Argonne Advanced Photon Source (APS) and Berkeley Lab Advanced Light Source (ALS). Data staging was performed with Globus endpoints running on dedicated data transfer nodes (DTNs) at each facility. All application I/O utilized each system’s production storage system (Lustre on Theta, IBM Spectrum Scale on Summit, and the project community filesystem (CFS) on Cori). The ALCF internal HTTPS proxy was used to enable outbound connections from the Theta application launch nodes to the Balsam service. Outbound HTTPS requests were directly supported from Cori and Summit compute nodes.

4.1.3 Applications. We chose two applications to measure throughput between facilities in multiple scenarios. The *matrix diagonalization* (MD) benchmark, which serves as a proxy for an arbitrary fine-grained numerical subroutine, entails a single Python NumPy call to the `eigh` function, which computes the eigenvalues and eigenvectors of a Hermitian matrix. The input matrix is transferred over the network from a client experimental facility and read from storage; after computation, the returned eigenvalues are written back to disk and transferred back to the requesting client’s local filesystem. We performed the MD benchmark with double-precision matrix sizes of 5000^2 (200 MB) and 12000^2 (1.15 GB), which correspond to eigenvalue (diagonal matrix) sizes of 40 kB and 96 kB, respectively. These sizes are representative of typical datasets acquired by the XPCS experiments discussed next.

The *X-ray photon correlation spectroscopy* (XPCS) technique presents a data-intensive workload in the study of nanoscale materials dynamics with coherent X-ray synchrotron beams, which is widely employed across synchrotron facilities such as the Advanced Photon Source (APS) at Argonne and the Advanced Light Source (ALS) at Lawrence Berkeley National Lab. In this case, we execute XPCS-Eigen [7] C++ package, used in the XPCS beamline, and the `corr` analysis which computes pixel-wise time correlations of area detector images of speckle patterns produced by hard X-ray scattering in a sample. The input comprises two files: a binary IMM file containing the sequence of acquired frames, and an HDF file containing experimental metadata and control parameters for the `corr` analysis routine. `corr` modifies the HDF file with results *in-place* and the file is subsequently transferred back to the Balsam client facility. For the study, we use an XPCS dataset comprised of 823 MB of IMM frames and 55 MB of HDF metadata. All the XPCS and MD runs herein were executed on a single compute node (i.e. without distributed-memory parallelism) and leverages OpenMP threads

scaling to the number of physical cores per node (64 on Theta, 42 on Summit, 32 on Cori).

4.1.4 Evaluation metrics. The Balsam service stores Balsam Job events (e.g. *job created*, *data staged-in*, *application launched*) with timestamps recorded at the job execution site. We leverage the Balsam API and Python analytics SDK to query this information and aggregate a variety of performance metrics:

- Throughput timelines for a particular job state (e.g. number of completed round-trip analyses as a function of time)
- Number of provisioned compute nodes and their instantaneous utilization (measured at the workflow level by number of running tasks)
- Latency incurred by each stage of the Balsam Job life-cycle

4.1.5 Local cluster baselines at experimental beamlines . For an experimental scientist, to understand the value of Balsam to offload analysis of locally acquired data, a key question to consider: *is the greater capacity of remotely distributed computing resources worth the cost of increased data transfer times and the time to solution?* We therefore aim to measure baseline performance in a pipeline that is characteristic of data analysis workflows executing on an HPC cluster near the data acquisition source as performed in production at the beamlines today[23]. In this case, the imaging data is first copied from the local acquisition machine storage to the beamline cluster storage and analysis jobs are launched next to analyze the data. To that end, we simulated “local cluster” scenarios on the Theta and Cori supercomputers by submitting MD benchmark runs continuously onto an exclusive reservation of 32 compute nodes and relying on the batch scheduler, not Balsam, to queue and schedule runs onto available resources. The reservations guaranteed resource availability during each run, so that measurements did not incur queuing delays due to other users on the system. Instead of using Globus Online to trigger data movement, transfers were invoked in the batch job script as file copy operations between a data source directory and a temporary sandbox execution directory on the same parallel filesystem.

4.2 Comparison to local cluster workflows

Figure 3 depicts the scalability of Balsam task throughput when remotely executing the MD application on Theta or Cori with input datasets stored at the APS. These measurements are compared with the throughput achieved by the “local cluster” pipeline, in which the same workload is repeatedly submitted onto an exclusive reservation of compute nodes via the local batch scheduler as described in section 4.1.5. We consider both Theta, which uses the Cobalt scheduler and Cori, which uses the Slurm scheduler. Note that on both machines, the Balsam workflow entails staging matrix data in from the APS Globus endpoint and transferring the output eigenvalues in the reverse direction back to APS. By contrast, the local cluster baseline does not include a wide area, cloud-mediated transfer and is therefore at an advantage in terms of reduced data transfer overhead. This is borne out in the “Stage In” and “Stage Out” histograms of figure 4, which show that local data movement times for the small (200 MB) MD benchmark are one to three orders of magnitude faster than the corresponding Globus transfers invoked by Balsam.

Despite added data transfer costs, Balsam efficiently overlaps asynchronous data movement with high-throughput task execution, yielding overall enhanced throughput and scalability relative to the local scheduler-driven workflows. On Theta, throughput increases from 4 to 32 nodes with 85% to 100% efficiency, depending on the sizes of transferred input datasets. On the other hand, the top panels of Figure 3 show that Cobalt-driven task throughput is non-scalable for the evaluated task durations on the order of 20 seconds (small input) or 1.5 minutes (large input). The Cobalt pipeline is in effect throttled by the scheduler job startup rate, with a median per-job queuing time of 273 seconds despite an exclusive reservation of idle nodes.

In contrast to Cobalt on Theta, the bottom panels of Figure 3 show that Slurm on Cori is moderately scalable for high-throughput workloads. For the smaller MD dataset, Slurm achieves 66% efficiency in scaling from 4 to 32 nodes; for the larger dataset efficiency increases to 85%. The improvement over Cobalt is due to the significantly reduced median Slurm job queuing delay of 2.7 seconds (see blue “Queueing” duration histograms in figure 4). Here too, Balsam scales with higher efficiency than the local baseline (87% for small dataset; 97% for large dataset), despite the wide geographic separation between the APS and NERSC facilities.

Provided adequate bandwidth, tapping remote resources clearly enables one to scale workloads beyond the capacity of local infrastructure, but this often comes at the price of unacceptably high turnaround time, with significant overheads in data movement and batch queuing. Table 1 quantifies the Balsam latency distributions that were measured from submitting 1156 small and 282 large MD tasks from APS to Theta at rates of 2.0 and 0.36 jobs/second, respectively. We note a mean 34.1 second overhead in processing the small MD dataset and 95th percentile overheads of roughly 1 or 2 minutes in processing the small or large MD datasets, respectively. On average, 84% to 90% of the overhead is due to data transfer time and not intrinsic to Balsam (which may, for instance, leverage direct memory-to-memory transfer methods). Notwithstanding room for improvement in transfer rates, turnaround times on the order of 1 minute may prove acceptable in *near-real-time* experimental scenarios requiring access to large-scale remote computing resources.

4.3 Optimizing the data staging

Figure 5 shows the effective cross-facility Globus transfer rates achieved in this work, summarized over a sample of 390 transfer tasks from the APS in which at least 10 GB of data were transmitted. We observed data rates from the APS to ALCF-Theta data transfer nodes were significantly lower than those to the OLCF and NERSC facilities, and needs further investigation. To adapt to various bandwidths and workload sizes, the Balsam site’s transfer module provides an adjustable *transfer batch size* parameter, which controls the maximum number of files per transfer task. When files are small relative to the available bandwidth, batching files is essential to leveraging the concurrency and pipelining capabilities of GridFTP processes underlying the Globus Transfer service [27]. On the other hand, larger transfer batch sizes yield diminishing returns on effective speed, increase the duration of transfer tasks,

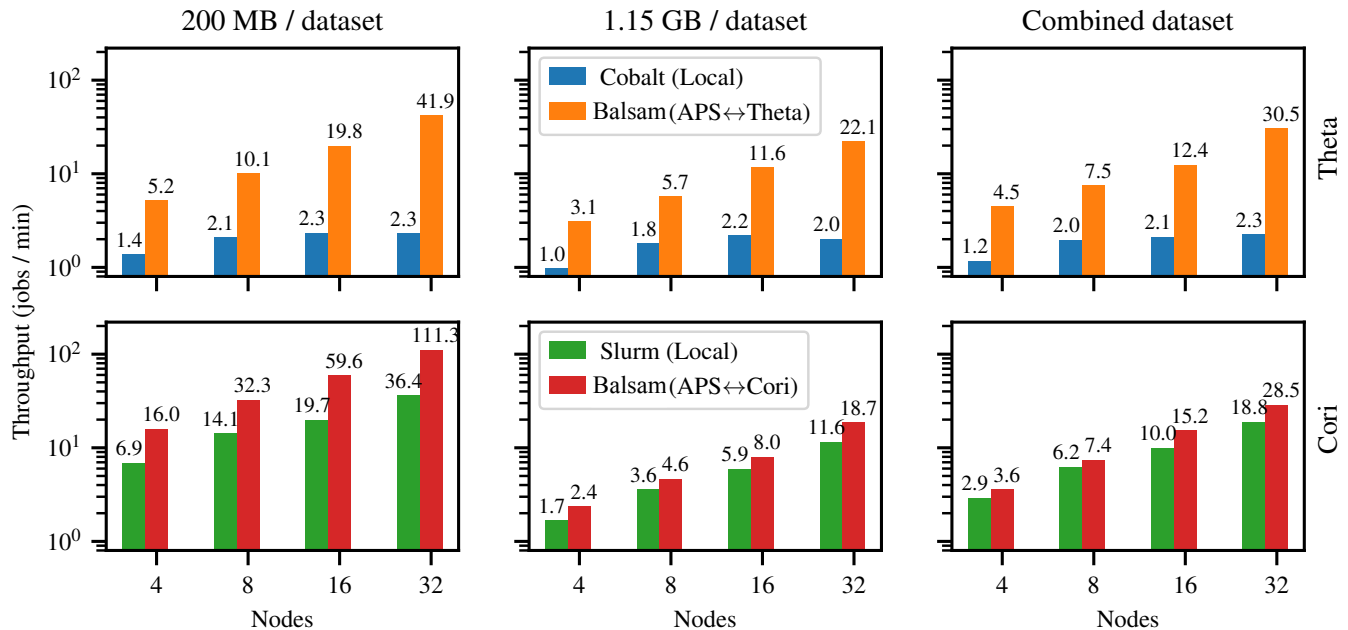


Figure 3: Weak scaling of matrix diagonalization throughput on Theta (top row) and Cori (bottom row). The average rate of task completion is compared between the local Batch Queue and Balsam APS \leftrightarrow ALCF/NERSC pipelines at various node counts. The left and center panels show runs using 5000^2 and 12000^2 input sizes, respectively. The right panels show runs in which each task submission draws uniformly at random from the two input sizes. To saturate Balsam data stage-in throughput, the job source throttled API submission to maintain a steady-state backlog of up to 48 datasets in flight. Up to 16 files were batched per Globus transfer task.

Table 1: APS \leftrightarrow Theta Balsam analysis pipeline stage durations (in seconds) for the matrix diagonalization benchmark. The latency incurred by each stage is reported as the mean \pm standard deviation, with the 95th percentile duration in parenthesis. Jobs were submitted to the Balsam API at a steady rate onto a 32-node allocation (2.0 and 0.36 jobs/second for the small and large datasets respectively).

Stage	200 MB (1156 runs) Duration (seconds)	1.15 GB (282 runs) Duration (seconds)
Stage In	17.1 \pm 3.8 (23.4)	47.2 \pm 17.9 (83.3)
Run Delay	5.3 \pm 11.5 (37.1)	7.4 \pm 14.7 (44.6)
Run	18.6 \pm 9.6 (30.4)	89.1 \pm 3.8 (95.8)
Stage Out	11.7 \pm 2.1 (14.9)	17.5 \pm 8.1 (34.1)
Time to Solution	52.7 \pm 17.6 (103.0)	161.1 \pm 23.8 (205.0)
Overhead	34.1 \pm 12.3 (66.3)	72.1 \pm 22.5 (112.2)

and may decrease opportunities for overlapping computation with smaller concurrent transfer tasks.

These tradeoffs are explored for the small and large MD datasets between the APS and a Theta Balsam site in Figure 6. As expected for the smaller dataset (each file is 200 MB), the aggregate job stage-in rate steadily improves with batch size, but then drops when batch size is set equal to the total workload size of 128 tasks. We attribute

this behavior to the limited default concurrency of 4 GridFTP processes *per transfer task*, which is circumvented by allowing Balsam to manage multiple smaller transfer tasks concurrently. For the larger MD dataset (each 1.15 GB), the optimal transfer batch size appears closest to 16 files.

4.4 Autoscaling and fault tolerance

The Balsam site provides an *elastic queueing* capability, which automates HPC queuing to provision resources in response to time-varying workloads. When job injection rates exceed the maximum attainable compute nodes in a given duration, Balsam durably accommodates the growing backlog and guarantees eventual execution in a fashion that is tolerant to faults at the Balsam service, site, launcher pilot job, or individual task level. Figure 7 shows the throughput and node utilization timelines of an 80-minute experiment between Theta and the APS designed to stress test these Balsam capabilities.

In the first phase (green background), a relatively slow API submission rate of 1.0 small MD job/second ensures that the completed application run count (green curve) closely follows the injected job count (blue curve) with an adequately-controlled latency. The gray trace in the bottom panel shows the number of available compute nodes quickly increasing to 32, obtained via four resource allocations in 8-node increments. As an aside, we mention that the node count and duration of batch jobs used to provision blocks of HPC

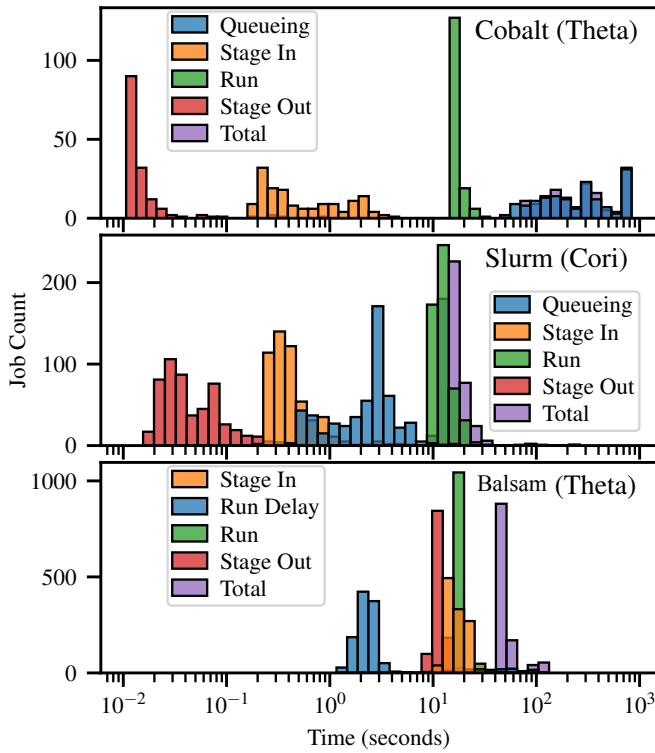


Figure 4: Histogram of latency contributions from stages in the Cobalt Batch Queuing (top), Slurm Batch Queuing (center), and APS ↔ Theta Balsam (bottom) analysis pipelines in the 200 MB matrix diagonalization benchmark. Jobs were submitted to the Balsam API at a steady rate of 2 jobs/second onto a 32-node allocation.

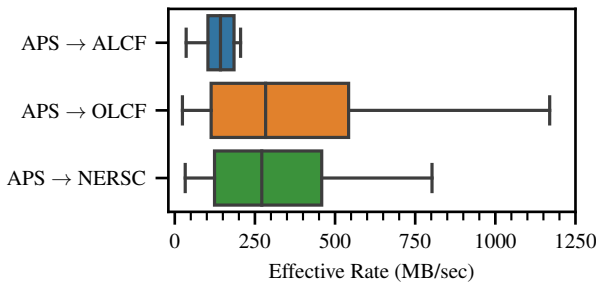


Figure 5: Effective cross-facility Globus transfer rates. The transfer duration is measured from initial API request to transfer completion; the rate therefore factors in average transfer task queue time and is lower than full end-to-end bandwidth. The boxes demarcate the quartiles of transfer rate to each facility, collected from 390 transfer tasks in which at least 10 GB were transmitted.

resources is adjustable within the Balsam site configuration. In fact, the elastic queuing module may opportunistically size jobs to fill idle resource gaps, using information provided by the local batch

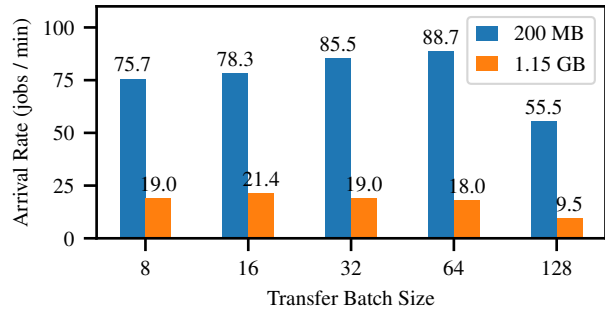


Figure 6: APS dataset arrival rate for matrix diagonalization benchmark on Theta, averaged over 128 Balsam Jobs. The Balsam site initiates up to three concurrent Globus transfers with a varying number of files per transfer (transfer batch size). For batch sizes of 64 and 128, the transfer is accomplished in only two (128/64) or one (128/128) Globus transfer tasks, respectively. The diminished rate at batch size 128 shows that at least two concurrent transfer tasks are needed to utilize the available bandwidth.

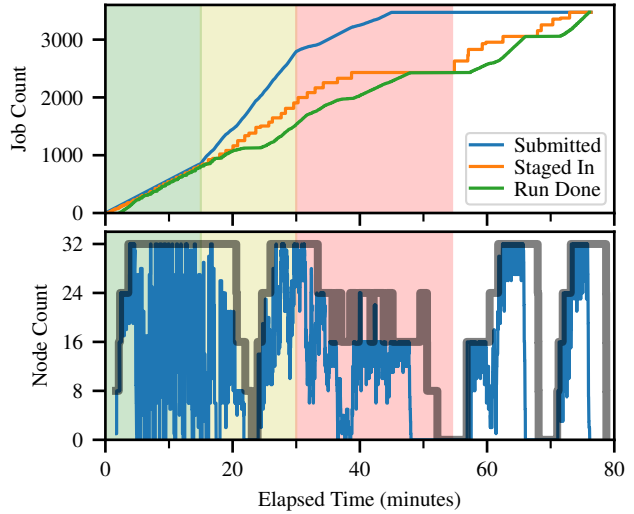


Figure 7: Elastic scaling during a Balsam stress test using the APS ↔ Theta matrix diagonalization benchmark with 200 MB dataset. Three traces in the top panel show the count of jobs submitted to the API, jobs for which the input dataset has been staged, and completed application runs. The bottom timeline shows the count of elastically-provisioned Theta compute nodes (gray) and count of running analysis tasks (blue). During the first 15 minutes (green region), jobs are submitted at a steady rate of 1.0 jobs/second. In the second 15 minutes (yellow region), jobs submitted at a rate of 3.0 jobs/second cause the task backlog to grow, because datasets arrive faster than can be handled with the maximum elastic scaling capacity (capped at 32 nodes for this experiment). In the third phase (red region), a randomly-chosen Balsam launcher is terminated every two minutes. In the final stage of the run, Balsam recovers from the faults to fully process the backlog of interrupted jobs.

scheduler. In this test, however, we fix the resource block size at 8 nodes and a 20 minutes maximum wall-clock time.

In the second phase (yellow background), the API submission rate triples from 1.0 to 3.0 small MD jobs/second. Meanwhile, the available node count briefly drops to 0, as the 20 minute limit expires for each of the initially allocated resource blocks. Application throughput recovers after the elastic queuing module provisions additional resources, but the backlog between submitted and processed tasks quickly grows larger. In the third phase (red background), we simulate faults in pilot job execution by *randomly terminating* one of the executing batch jobs every two minutes, thereby causing up to 8 MD tasks to timeout. The periodically killed jobs, coupled with large scheduler startup delays on Theta, causes the number of available nodes to fluctuate between 16 and 24. Additionally, the Balsam site experiences a stall in Globus stage-ins, which exhausts the runnable task backlog and causes the launchers to time-out on idling. Eventually, in the fourth and final region, the adverse conditions are lifted, and Balsam processes the full backlog of tasks across several additional resource allocations. We emphasize that no tasks are lost in this process, as the Balsam service durably tracks task states in its relational database and monitors the heartbeat from launchers to recover tasks from ungracefully-terminated sessions. These features will enable us robustly support the bursty workloads in experimental workloads as well as the ability to provide fault-tolerant computational infrastructure to the real-time experiments.

4.5 Simultaneous execution on geographically distributed supercomputers

We evaluate the efficacy of Balsam in distributing XPCS (section 4.1.3) workloads from one or both of the APS and ALS national X-ray facilities on to the Theta, Cori and Summit supercomputing systems in real time. By starting Balsam sites on the login (or gateway or service) nodes of three supercomputers, a user transforms these independent facilities into a federated infrastructure with uniform APIs and a Python SDK to securely orchestrate the life-cycle of geographically-distributed HPC workflows.

Figure 8 shows the median time spent in each stage of a remote Balsam XPCS corr analysis task execution with 878 MB dataset. The overall time-to-solution, from task submission to returned calculation results, ranges from 86 seconds (APS \leftrightarrow Cori) to a maximum of 150 seconds (ALS \leftrightarrow Theta). These measurements were performed with an allocation of 32 nodes on each supercomputer and without pipelining input data transfers, thereby minimizing latency in Globus transfer task queuing and application startup time. From Figure 8 it is clear that data transfer times dominate the remote execution overheads consisting of stage in, run delay and stage out. However, these overheads are within the constraints needed for near-real-time execution. We emphasize that there is significant room for network performance optimizations and opportunities to interface the Balsam transfer service with performant alternatives to disk-to-disk transfers. Moreover, the overhead in Balsam application launch itself is consistently in the range of 1 to 2 seconds (1% to 3% of XPCS runtime, depending on the platform).

Figure 9 charts the simultaneous throughput of XPCS analyses executing concurrently on 32 compute nodes of each system: Theta,

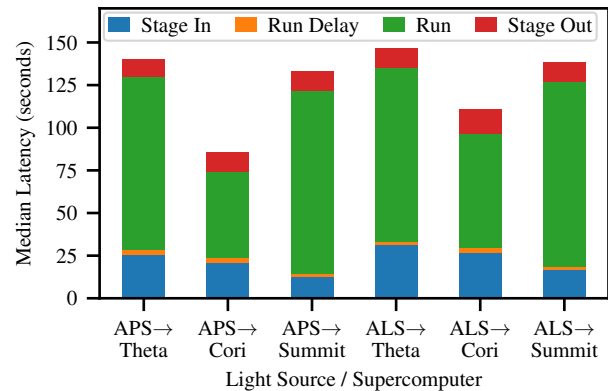


Figure 8: Contribution of stages in the Balsam Job life-cycle to total XPCS analysis latency. With at most one 878 MB dataset in flight to each compute facility, the bars reflect round-trip time to solution in the absence of pipelining or batching data transfers. The green *Run* segments represent the median runtime of the XPCS-Eigen corr calculation. The blue and red segments represent overheads in Globus data transfers. Orange segment represents the delay in Balsam application startup after input dataset has been staged.

Cori, and Summit. The three panels correspond to separate experiments in which (1) XPCS is invoked from APS datasets alone, (2) XPCS is invoked from ALS datasets alone, or (3) XPCS is invoked with a randomly selected dataset from either APS or ALS. To measure the attainable throughput in each scenario, the clients varied submission rate to maintain a *steady-state backlog* of 32 XPCS tasks: that is, the sum of submitted and staged-in (but not yet running) tasks fluctuates near 32 for each system. The Balsam site transfer batch size was set to a maximum of 32 files per transfer, and each site initiated up to 5 concurrent transfer tasks. On the Globus service backend, this implies up to 3 *active* and 12 *queued* transfer tasks at any moment in time. In practice, the stochastic arrival rates and interwoven stage-in and result stage-out transfers reduce the file count per transfer task.

One immediately observes a consistent ordering in throughput increasing from Theta \rightarrow Summit \rightarrow Cori, regardless of the client light source. The markedly improved throughput on Cori relative to other systems is mainly due to reduced application runtime, which is clearly evident from Figure 8. While the throughput of Theta and Summit are roughly on-par, Summit narrowly though consistently outperforms Theta due to higher effective stage-in throughput bandwidth. This is evident in the *top boundary* of the orange and blue regions of Figure 9, which show the arrival throughput of staged-in datasets. Indeed, the average XPCS arrival rates calculated from the APS experiment (left panel) are 16.0 datasets/minute for Theta, 19.6 datasets/minute for Summit, and 29.6 datasets/minute for Cori. We also notice that Cori's best data arrival rate is inconsistent with the slower median stage in time of Figure 8. Because those durations were measured without batching file transfers, this underscores the significance of GridFTP pipelining and concurrency on the Cori data transfer nodes.

Continuing our analysis of Figure 9, the *center line* in each colored region shows the throughput of completed application runs,

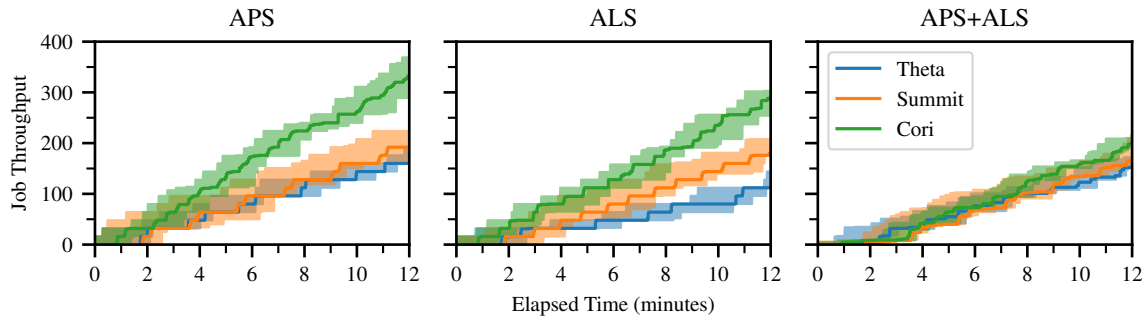


Figure 9: Simultaneous throughput of XPCS analysis on Theta (blue), Summit (orange), and Cori (green) Balsam sites. The panels (left to right) correspond to experiments in which the 878 MB XPCS dataset is transferred from either the APS, ALS, or both light sources. A constant backlog of 32 tasks was maintained with the Balsam API. The top boundary of each shaded region shows the number of staged-in datasets. The center line shows the number of completed application runs. The bottom boundary of the shaded regions shows the number of staged-out result sets. When the center line approaches the top of the shaded region, the system is network I/O-bound: that is, compute nodes become idle waiting for new datasets to arrive.

which naturally lags behind the staged-in datasets by the XPCS application’s running duration. Similarly, the *bottom boundary* of each colored region shows the number of completed result transfers back to the client; the gap between the center line and bottom of the region represents the “Stage Out” portion of each pipeline. The XPCS results comprise only the HDF file, which is modified in-place during computation and (at least) an order-of-magnitude smaller than the IMM frame data. Therefore, result transfers tend to track application completion more closely, which is especially noticeable on Summit.

When the center line in a region of Figure 9 approaches or intersects the top region boundary, the number of *completed* application runs approaches or matches the number of *staged-in* XPCS datasets. In this scenario, the runnable workload on a supercomputer becomes too small to fill the available 32 nodes: in effect, the system is network I/O-bound. The compute utilization percentages in Figure 10 make this abundantly clear for the APS experiment. On Summit, the average arrival rate of 19.6 datasets/minute and 108 second application runtime are sufficiently high to keep all resources busy. Indeed, for Summit both the instantaneous utilization measured from Balsam event logs (blue curve) and its time-average (dashed line) remain very close to 100% (32/32 nodes running XPCS analysis at all times).

We can apply Little’s law [24] in this context, an intuitive result from queuing theory which states that the long-run average number L of running XPCS tasks should be equal to the product of average effective dataset arrival rate λ and application runtime W . We thus compute the empirical quantity $L = \lambda W$ and plot it in Figure 10 as the semi-transparent thick yellow line. The close agreement between time-averaged node utilization and the expected value λW helps us to estimate the *potential headroom for improvement of throughput* by increasing data transfer rates (λ). For example, even though APS \leftrightarrow Cori achieves better overall throughput than APS \leftrightarrow Summit (Figure 9), we see that Cori reaches only about 75% of its sustained XPCS processing capacity at 32 nodes, whereas Summit is near 100% utilization and therefore compute-bound (of course barring optimizations in application I/O or other acceleration techniques at the task level). Furthermore, Figure 8 shows that XPCS application runtime on Theta is comparable to Summit, but Theta

has a significantly slower arrival rate. This causes lower average utilization of 76% on Theta.

Overall, by using Balsam to scale XPCS workloads from the APS across three distributed HPC systems simultaneously, we achieved 4.37-fold increased throughput over the span of a 19-minute run compared to routing workloads to Theta alone (1049 completed tasks in aggregate, versus 240 tasks completed on Theta alone). Similarly, we achieve a 3.28X improvement in throughput over Summit and 2.2X improvement over Cori. This demonstrates the importance of utilizing geographically distributed supercomputing sites to meet the needs of real-time analysis of experiments for improved time to solution. We note that the Globus Transfer default limit of 3 concurrent transfer tasks per user places a significant constraint on peak throughput achievable by a single user. This issue is particularly evident in the right-most panel of Figure 9, where Balsam is managing bi-directional transfers along six routes. As discussed earlier, the clients in this experiment throttled submission to maintain a *steady backlog* of 32 jobs per site. Splitting this backlog in half between two remote data sources (APS and ALS) decreases opportunities for batching transfers and reduces overall benefits of pipelining/concurrency in file transfers. Of course, this is to some extent an artifact of the experimental design: real distributed clients would likely use different Globus user accounts and would *not* throttle task injection to maintain a steady backlog. Nevertheless, increasing concurrency limits on data transfers could provide significant improvements in global throughput where many Balsam client–execution site endpoint pairs are concerned.

4.6 Adaptive workload distribution

The previous section focused on throughputs and latencies in the Balsam distributed system for analysing XPCS data on Theta, Summit, and Cori execution sites. We now relax the artificial *steady backlog* constraint and instead allow the APS client to inject workloads in a more realistic fashion: jobs are submitted at a *constant average rate* of 2.0 jobs/second, spread across batch-submission blocks of 16 XPCS jobs every 8.0 seconds. This workload represents a plausible experimental workflow, in which 14 GB batches of data (16 datasets \times 878 MB/dataset) are periodically collected and dispatched for

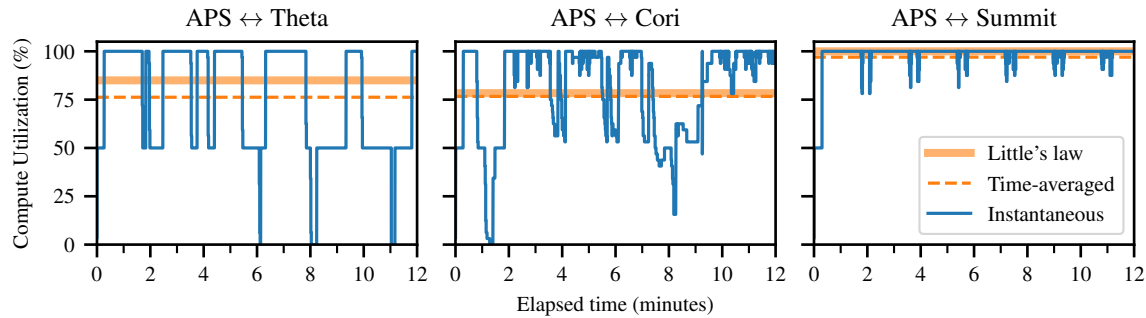


Figure 10: Compute node utilization on each Balsam site corresponding to the APS experiment in Figure 9. The solid line shows the instantaneous node utilization, measured via Balsam events as a percentage of the full 32-node reservation on each system. The dashed line indicates the time-averaged utilization, which should coincide closely with the *expected* utilization derived from the average data arrival rate and application runtime (Little’s law). The data arrival rate on Summit is sufficiently high that compute nodes are busy near 100% of the time. By contrast, Theta and Cori reach about 75% utilization due to a bottleneck in effective data transfer rate.

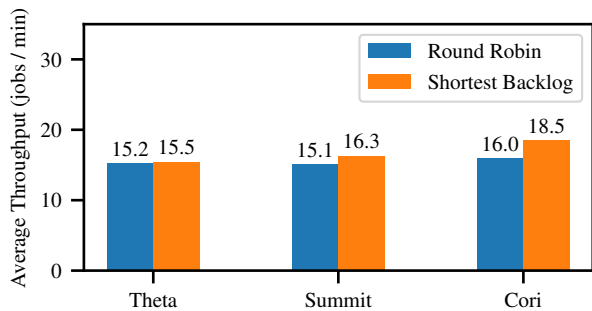


Figure 11: Throughput of client-driven task distribution strategies for the XPCS benchmark with APS data source. Using round-robin distribution, XPCS jobs are evenly distributed alternating among the three Balsam sites. Using the shortest-backlog strategy, the client uses the Balsam API to adaptively send jobs to the site with the smallest pending workload. In both scenarios, the client submits a batch of 16 jobs every 8 seconds.

XPCS-Eigen analysis remotely. It also introduces a scheduling problem, wherein the client may naively distribute workloads evenly among available execution sites (round-robin) or leverage the Balsam Job events API to *adaptively* route tasks to the system with shortest backlog, lowest estimated time-to-solution, etc... Here, we explore a simplified variant of this problem, where XPCS tasks are uniformly-sized and each Balsam site has a constant resource availability of 32 nodes.

Figure 11 compares the average throughput of XPCS dataset analysis from the APS when distributing work according to one of two strategies: *round-robin* or *shortest-backlog*. In the latter strategy, the client uses the Balsam API to poll the number of jobs pending stage-in or execution at each site; the client then submits each XPCS batch to the Balsam site with the shortest backlog in a first-order load-levelling attempt. We observed a slight 16% improvement in throughput on Cori when using the shortest-backlog strategy relative to round-robin, with marginal differences for Theta and Summit. The submission rate of 2.0 jobs/second or 120 jobs/minute significantly exceeds the aggregate sustained throughput of approximately 58 jobs/minute seen in the left panel of Figure 9. We

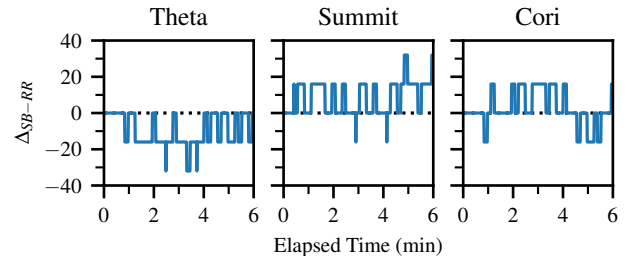


Figure 12: Difference in per-site job distribution between the considered strategies. Each curve shows the instantaneous difference in submitted task count between the shortest-backlog and round-robin strategies (Δ_{SB-RR}) over the span of six minutes of continuous submission. A negative value indicates that *fewer* jobs were submitted at the same point in time during the round-robin run, relative to the shortest-backlog run.

therefore expect a more significant difference between the distribution strategies when job submission rates are balanced with the attainable system throughput.

Nevertheless, Figure 12 shows that with the shortest-backlog strategy, the APS preferentially submits more workloads to Summit and Cori, and fewer workloads to Theta, which tends to accumulate backlog more quickly owing to slower data transfer rates. This results in overall increased data arrival rates and higher throughput on Cori (Figure 11), despite overloaded pipelines on all three systems.

5 CONCLUSION

In this work, we describe the Balsam workflow framework to enable wide-area, multi-tenant, distributed execution of analysis jobs on DOE supercomputers. A key development is the introduction of a central Balsam service that manages job distribution, fronted by a programmatic interface. Clients of this service use the API to inject jobs, and to control and monitor their execution; these clients reside anywhere, on a user’s laptop or on institutional clusters, opening

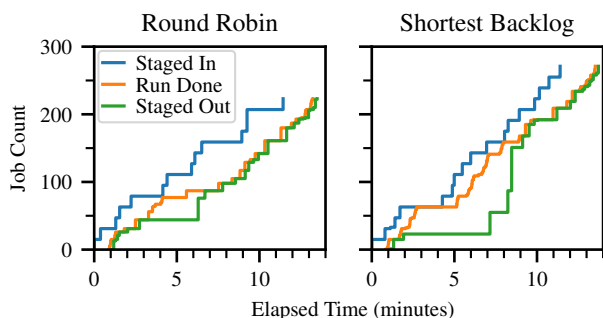


Figure 13: Throughput of data staging and application runs on Cori, compared between round-robin and shortest-backlog strategies. More frequent task submissions to Cori in the adaptive shortest-backlog strategy contribute to 16% higher throughput relative to round-robin strategy.

new opportunities for interfacing with large-scale computing facilities. A second key development is another type of client, a Balsam site, which consumes jobs from the Balsam service and interacts directly with the scheduling infrastructure of a cluster. Together, these two form a distributed, multi-resource execution landscape.

The power of this approach was demonstrated using the Balsam API to inject analysis jobs from two light source facilities to the Balsam service, targeting simultaneous execution on three DOE supercomputers. By strategically combining data transfer bundling and controlled job execution, Balsam achieves higher throughput than direct-scheduled local jobs and effectively balances job distribution across sites to simultaneously utilize multiple remote supercomputers. Utilizing three geographically distributed supercomputers concurrently, we achieve a 4.37-fold increased throughput compared to routing light source workloads to Theta, a 3.28X improvement in throughput over Summit and 2.2X improvement over Cori. Balsam enables the combined power of these facilities to be brought to bare on experimental workloads with an improved resiliency that comes from dynamically adapting to compute availability across multiple sites. Other key results include that Balsam is a user-domain solution that can be deployed without administrative support, while honoring the security constraints of facilities; that Balsam overhead is minimal relative to job runtimes and data transfer time; and the introduction of elastic scaling in Balsam, to utilize additional nodes to meet increasing workload availability.

ACKNOWLEDGMENT

This work was funded in part and used resources of the Argonne Leadership Computing Facility at Argonne National Laboratory, a DOE Office of Science User Facility supported under Contract DE-AC02-06CH11357.

The submitted manuscript has been created by UChicago Argonne, LLC, Operator of Argonne National Laboratory (“Argonne”). Argonne, a U.S. Department of Energy Office of Science laboratory, is operated under Contract No. DE-AC02-06CH11357. The U.S. Government retains for itself, and others acting on its behalf, a paid-up nonexclusive, irrevocable worldwide license in said article to reproduce, prepare derivative works, distribute copies to the public, and perform publicly and display publicly, by or on behalf of the Government.

REFERENCES

- [1] [n.d.]. Cori. <https://docs.nersc.gov/systems/cori/#haswell-compute-nodes>.
- [2] [n.d.]. Globus Online. <https://www.globus.org>.
- [3] [n.d.]. OAuth 2.0 Device Authorization Grant. <https://tools.ietf.org/html/rfc6828>
- [4] [n.d.]. PostgreSQL. <https://www.postgresql.org/>
- [5] [n.d.]. Summit. <https://www.olcf.ornl.gov/olcf-resources/compute-systems/summit/>
- [6] [n.d.]. Theta. <https://www.alcf.anl.gov/alcf-resources/theta>.
- [7] [n.d.]. XPCS-Eigen. <https://github.com/AdvancedPhotonSource/xpcs-eigen>.
- [8] Malcolm Atkinson, Sandra Gesing, Johan Montagnat, and Ian Taylor. 2017. Scientific workflows: Past, present and future. *Future Generation Computer Systems* 75 (Oct. 2017), 216–227. <https://doi.org/10.1016/j.future.2017.05.041>
- [9] Yadu Babuji, Anna Woodard, Zhuozhao Li, Daniel S. Katz, Ben Clifford, Rohan Kumar, Luksaz Lacinski, Ryan Chard, Justin M. Wozniak, Ian Foster, Michael Wilde, and Kyle Chard. 2019. Parsl: Pervasive-Parallel Programming in Python. In *28th ACM International Symposium on High-Performance Parallel and Distributed Computing (HPDC)*. <https://doi.org/10.1145/3307681.3325400> babuji19parsl.pdf
- [10] V. Balasubramanian, A. Treikalis, O. Weidner, and S. Jha. 2016. Ensemble Toolkit: Scalable and Flexible Execution of Ensembles of Tasks. In *2016 45th International Conference on Parallel Processing (ICPP)*. IEEE Computer Society, Los Alamitos, CA, USA, 458–463. <https://doi.org/10.1109/ICPP.2016.59>
- [11] Krzysztof Burkat, Maciej Pawlik, Bartosz Balis, Maciej Malawski, Karan Vahi, Mats Rynge, Rafael Ferreira da Silva, and Ewa Deelman. 2020. Serverless Containers – rising viable approach to Scientific Workflows. arXiv:2010.11320 [cs.DC]
- [12] Joseph Carlson, Martin J. Savage, Richard Gerber, Katie Antypas, Deborah Bard, Richard Coffey, Eli Dart, Sudip Dossanjh, James Hack, Inder Monga, Michael E. Papka, Katherine Riley, Lauren Rotman, Tjerk Straatsma, Jack Wells, Harut Avakian, Yassid Ayyad, Steffen A. Bass, Daniel Bazin, Amber Boehnlein, Georg Bollen, Leah J. Broussard, Alan Calder, Sean Couch, Aaron Couture, Mario Cromaz, William Detmold, Jason Detwiler, Huaiyu Duan, Robert Edwards, Jonathan Engel, Chris Fryer, George M. Fuller, Stefano Gandolfi, Gagik Gavalian, Dali Georgobiani, Rajan Gupta, Vardan Gyurjyan, Marc Hausmann, Graham Heyes, W. Ralph Hix, Mark Ito, Gustav Jansen, Richard Jones, Balint Joo, Olaf Kaczmarek, Dan Kasen, Mikhail Kostin, Thorsten Kurth, Jerome Laurent, David Lawrence, Huey-Wen Lin, Meifeng Lin, Paul Mantica, Peter Maris, Bronson Messer, Wolfgang Mittag, Shea Mosby, Swagato Mukherjee, Hai Ah Nam, Petr navratil, Witek Nazarewicz, Esmond Ng, Tommy O’Donnell, Konstantinos Orginos, Frederique Pellemoine, Peter Petreczky, Steven C. Pieper, Christopher H. Pinkenburg, Brad Plaster, R. Jefferson Porter, Mauricio Portillo, Scott Pratt, Martin L. Purschke, Ji Qiang, Sofia Quagliioni, David Richards, Yves Roblin, Bjorn Schenke, Rocco Schiavilla, Soren Schlichting, Nicolas Schunck, Patrick Steinbrecher, Michael Strickland, Sergey Syritsyn, Balsa Terzic, Robert Varner, James Vary, Stefan Wild, Frank Winter, Remco Zegers, He Zhang, Veronique Ziegler, and Michael Zingale. 2017. Nuclear Physics Exascale Requirements Review: An Office of Science review sponsored jointly by Advanced Scientific Computing Research and Nuclear Physics, June 15 - 17, 2016, Gaithersburg, Maryland. (2 2017). <https://doi.org/10.2172/1369223>
- [13] Ryan Chard, Yadu Babuji, Zhuozhao Li, Tyler Skluzacek, Anna Woodard, Ben Blaiszik, Ian Foster, and Kyle Chard. 2020. funcX: A Federated Function Serving Fabric for Science. *Proceedings of the 29th International Symposium on High-Performance Parallel and Distributed Computing*. <https://doi.org/10.1145/3369583.3392683>
- [14] Dask Development Team. 2016. *Dask: Library for dynamic task scheduling*. <https://dask.org>
- [15] B. Enders, D. Bard, C. Snavely, L. Gerhardt, J. Lee, B. Totzke, K. Antypas, S. Byna, R. Cheema, S. Cholia, M. Day, A. Gaur, A. Greiner, T. Groves, M. Kiran, Q. Koziol, K. Rowland, C. Samuel, A. Selvarajan, A. Sim, D. Skinner, R. Thomas, and G. Torok. 2020. Cross-facility science with the Superfacility Project at LBNL. In *2020 IEEE/ACM 2nd Annual Workshop on Extreme-scale Experiment-in-the-Loop Computing (XLOOP)*. IEEE Computer Society, Los Alamitos, CA, USA, 1–7. <https://doi.org/10.1109/XLOOP51963.2020.00006>
- [16] Salman Habib, Robert Roser, Richard Gerber, Katie Antypas, Katherine Riley, Tim Williams, Jack Wells, Tjerk Straatsma, A. Almgren, J. Arundson, S. Bailey, D. Bard, K. Bloom, B. Bockelman, A. Borgland, J. Borrill, R. Boughezal, R. Brower, B. Cowan, H. Finkel, N. Frontiere, S. Fuess, L. Ge, N. Gnedin, S. Gottlieb, O. Gutsche, T. Han, K. Heitmann, S. Hoeche, K. Ko, O. Kononenko, T. LeCompte, Z. Li, Z. Lukic, W. Mori, P. Nugent, C. K. Ng, G. Oleynik, B. O’Shea, N. Padmanabhan, D. Petravick, F. J. Petriello, J. Power, J. Qiang, L. Reina, T. J. Rizzo, R. Ryne, M. Schram, P. Spentzouris, D. Toussaint, J. L. Vay, B. Viren, F. Wurthwein, and L. Xiao. 2017. ASCR/HEP Exascale Requirements Review Report. (2 2017). <https://www.osti.gov/biblio/1398463>
- [17] Anubhav Jain, Shyue Ping Ong, Wei Chen, Bharat Medasani, Xiaohui Qu, Michael Kocher, Miriam Brafman, Guido Petretto, Gian-Marco Rignanes, Geoffroy Hautier, Daniel Gunter, and Kristin A. Persson. 2015. FireWorks: a dynamic workflow system designed for high-throughput applications. *Concurrency and Computation: Practice and Experience* 27, 17 (2015), 5037–5059. <https://doi.org/10.1002/cpe.3505> CPE-14-0307.R2.

- [18] M. Salim, T. Uram, J. T. Childers, V. Vishwanath, and M. Papka. 2019. Balsam: Near Real-Time Experimental Data Analysis on Supercomputers. In *2019 IEEE/ACM 1st Annual Workshop on Large-scale Experiment-in-the-Loop Computing (XLOOP)*. 26–31. <https://doi.org/10.1109/XLOOP49562.2019.00010>
- [19] Mallikarjun (Arjun) Shankar and Eric Lancon. 2019. *Background and Roadmap for a Distributed Computing and Data Ecosystem*. Technical Report. <https://doi.org/10.2172/1528707>
- [20] Joe Stubbs, Suresh Marru, Daniel Mejia, Daniel S. Katz, Kyle Chard, Maytal Dahan, Marlon Pierce, and Michael Zentner. 2020. Toward Interoperable Cyberinfrastructure: Common Descriptions for Computational Resources and Applications. In *Practice and Experience in Advanced Research Computing*. ACM. <https://doi.org/10.1145/3311790.3400848>
- [21] S Timm, G Cooper, S Fuess, G Garzoglio, B Holzman, R Kennedy, D Grassano, A Tiradani, R Krishnamurthy, S Vinayagam, I Raicu, H Wu, S Ren, and S-Y Noh. 2017. Virtual machine provisioning, code management, and data movement design for the Fermilab HEPcloud Facility. *Journal of Physics: Conference Series* 898 (oct 2017), 052041. <https://doi.org/10.1088/1742-6596/898/5/052041>
- [22] T D Uram, J T Childers, T J LeCompte, M E Papka, and D Benjamin. 2015. Achieving production-level use of HEP software at the Argonne Leadership Computing Facility. *Journal of Physics: Conference Series* 664, 6 (dec 2015), 062063. <https://doi.org/10.1088/1742-6596/664/6/062063>
- [23] Siniša Veseli, Nicholas Schwarz, and Collin Schmitz. 2018. APS Data Management System. *Journal of Synchrotron Radiation* 25, 5 (Aug. 2018), 1574–1580. <https://doi.org/10.1107/s1600577518010056>
- [24] Wikipedia contributors. 2021. Little’s law. [https://en.wikipedia.org/wiki/Little’s law](https://en.wikipedia.org/wiki/Little%27s_law) [Online; accessed 22-July-2004].
- [25] Michael Wilde, Mihael Hategan, Justin M. Wozniak, Ben Clifford, Daniel S. Katz, and Ian Foster. 2011. Swift: A language for distributed parallel scripting. *Parallel Comput.* 37, 9 (2011), 633–652. <https://doi.org/10.1016/j.parco.2011.05.005>
- Emerging Programming Paradigms for Large-Scale Scientific Computing.
- [26] Theresa Windus, Michael Banda, Thomas Devereaux, Julia C. White, Katie Antypas, Richard Coffey, Eli Dart, Sudip Dosanjh, Richard Gerber, James Hack, Inder Monga, Michael E. Papka, Katherine Riley, Lauren Rotman, Tjerk Straatsma, Jack Wells, Tunna Baruah, Anouar Benali, Michael Borland, Jiri Brabec, Emily Carter, David Ceperley, Maria Chan, James Chelikowsky, Jackie Chen, Hai-Ping Cheng, Aurora Clark, Pierre Darancet, Wibe DeJong, Jack Deslippe, David Dixon, Jeffrey Donatelli, Thomas Dunning, Marivi Fernandez-Serra, James Freericks, Laura Gagliardi, Giulia Galli, Bruce Garrett, Vassiliki-Alexandra Glezakou, Mark Gordon, Niri Govind, Stephen Gray, Emanuel Gull, Francois Gygi, Alexander Hexemer, Christine Isborn, Mark Jarrell, Rajiv K. Kalia, Paul Kent, Stephen Klippenstein, Karol Kowalski, Hulikal Krishnamurthy, Dinesh Kumar, Charles Lena, Xiaosong Li, Thomas Maier, Thomas Markland, Ian McNulty, Andrew Millis, Chris Mundy, Aiichiro Nakano, A.M.N. Niklasson, Thanos Panagiotopoulos, Ron Pandolfi, Dula Parkinson, John Pask, Amedeo Perazzo, John Rehr, Roger Rousseau, Subramanian Sankaranarayanan, Greg Schenter, Annabella Selloni, Jamie Sethian, Ilja Siepmann, Lyudmila Slipchenko, Michael Sternberg, Mark Stevens, Michael Summers, Bobby Sumpter, Peter Sushko, Jana Thayer, Brian Toby, Craig Tull, Edward Valeev, Priya Vashishta, V. Venkatakrishnan, C. Yang, Ping Yang, and Peter H. Zwart. 2017. Basic Energy Sciences Exascale Requirements Review. An Office of Science review sponsored jointly by Advanced Scientific Computing Research and Basic Energy Sciences, November 3-5, 2015, Rockville, Maryland. (2 2017). <https://doi.org/10.2172/1341721>
- [27] Esma Yildirim, JangYoung Kim, and Tefik Kosar. 2012. How GridFTP Pipelining, Parallelism and Concurrency Work: A Guide for Optimizing Large Dataset Transfers. In *2012 SC Companion: High Performance Computing, Networking Storage and Analysis*. IEEE. <https://doi.org/10.1109/sc.companion.2012.73>